Journal of Physics: Conference Series **635** (2015) 012007 doi:10.1088/1742-6596/635/1/012007

On time-resolved electron emission at the attosecond time scale

C.-Z. Gao[a,b], P. M. Dinh[a,b], P.-G. Reinhard[c], E. Suraud[a,b]

[a]Université de Toulouse, UPS; Laboratoire de Physique Théorique (IRSAMC), F-31062 Toulouse Cedex, France
[b]CNRS; LPT (IRSAMC), Université de Toulouse, F-31062 Toulouse Cedex, France
[c]Institut für Theoretische Physik, Universität Erlangen, D-91058 Erlangen, Germany

E-mail: gao@irsamc.ups-tlse.fr

Abstract. We investigate from a theoretical perspective time-resolved photoionization of N_2 irradiated by a combination of a long infrared (IR) pulse with a dedicated train of attosecond pulses (APT) in the extreme ultraviolet (XUV) range. The delay time of the attosecond train with respect to the infrared pulse is systematically varied, in accordance with experiments. We find marked oscillations of the ionization yield as a function of delay. We analyze the position of maxima and minima of electron yield and trends with XUV frequency.

1. Introduction

Exploring the structure and dynamics of molecules and clusters has been one of longstanding interests in many fields of science. Lasers provide invaluable probes of the properties of these systems in a time-resolved manner. Ultrashort and ultrafast laser technology for molecular dynamics has been marked by femtosecond pulses [1], which provide a nanometric imaging of chemical reactions as well as a femtosecond time resolution of transition states. More recently, high harmonic generations (HHG) from an intense near infra-red (NIR) laser pulse are experimentally used for the construction of attosecond pulse trains (APT) [2]. The NIR pump - APT probe setup is extensively used to trigger, monitor, and manipulate electronic motions in various experiments [3, 4, 5, 6]. To explain and understand the numerous measurements, different theoretical models have been developed. For small systems, such as H and He atoms, it is possible to exactly solve the time-dependent Schrödinger equation and to compute related observables as, e.g., photo-electron spectra (PES). For systems with a larger number of electrons occupying distinct orbitals, the single-active electron approximation [7], which neglects any other electron's dynamics, can shed light on experimental results both qualitatively and quantitatively in some cases. Another approach consists in Time-Dependent Density-Functional Theory (TDDFT) [8] for the description of valence electrons dynamics, coupled non-adiabatically to molecular dynamics for the ionic motion [9]. In this paper, we apply TDDFT to the study of electron emission from the N_2 molecule, irradiated by a NIR-APT laser setup, and we focus in particular on the effect of laser polarization, ionic motion, and the XUV frequency of APT.

The paper is outlined as follows. In Section 2, the theoretical model and numerical details are briefly introduced. Results are discussed in Section 3. Finally, a summary is drawn in Section 4.

2. Theoretical approach

In the framework of TDDFT, the dynamics of the $N_{\rm el}$ valence electrons is treated at the level of Time-Dependent Local-Density Approximation (TDLDA) [10] augmented by an average-density self-interaction correction [11]. The latter correction ensures a correct asymptotic decay of the Kohn-Sham (KS) potential which is critical for a pertinent description of electron emission [12]. We consider here the 5 valence electrons of the N atom, while core electrons are coupled to valence electrons via Goedecker-like pseudo-potentials [13]. The motion of the N^{5+} ionic cores is described by molecular dynamics, non-adiabatically coupled to TDDFT [9].

The laser interaction is treated in the dipole approximation. We here consider a combination of a NIR laser pump and an APT probe, both polarized along the same direction [14] :

$$E_{\rm ext}(t) = E_{\rm NIR}(t) + E_{\rm atto}(t) \ , \tag{1}$$

$$E_{\rm NIR}(t) = E_0^{\rm (NIR)} \sin(\omega_{\rm NIR} t)\, f_{T_{\rm NIR}}(t) \ , \tag{2}$$

$$E_{\rm atto}(t) = E_0^{\rm (atto)} \sin(\omega_{\rm atto} t)\, g(t) \sum_{\alpha=0}^{N-1} f_{T_{\rm atto}}\left(t - (\Delta\tau + \alpha T_{\rm train})\right) \ , \tag{3}$$

where f_T is a pulse envelope which reads :

$$f_T(t) = \sin^2\left(\frac{t}{T}\pi\right)\theta(t)\theta(T-t) \ . \tag{4}$$

θ stands for the Heaviside function. The NIR laser pulse is characterized by a wavelength of 800 nm (i.e., $\omega_{\rm NIR} = 1.55$ eV) and a total pulse duration $T_{\rm NIR} = 60$ fs. Its field strength $E_0^{\rm (NIR)}$ corresponds to an intensity of 10^{12} W/cm^2. The APT consists in a succession of $N = 21$ attopulses of width $T_{\rm atto} = 0.3$ fs. The amplitude of the train is modulated by the Gaussian envelope g, see Eq. (3), centered at $\Delta\tau + NT_{\rm train}/2$ and having a half-width of $NT_{\rm train}/2$. This Gaussian profile is the same as that used in the experiment of [15]. The time separation between the attopulses in the train is equal to half a period of the NIR pulse, i.e., $\pi/\omega_{\rm NIR}$. The field strength $E_0^{\rm (atto)}$ of the APT corresponds to an intensity of 10^9 W/cm^2. A key parameter is the delay time $\Delta\tau$. It determines the phase along the NIR pulse at which the APT starts [3, 4]. In the following, we always use pulses with the parameters given above. Only the delay time $\Delta\tau$ and the frequency of the attopulses $\omega_{\rm atto}$ are varied.

Calculations are performed on a tridimensional coordinate-space grid [9, 16]. Occasionally, a cylindrically averaged pseudopotential scheme (CAPS) is used [17]. The CAPS imposes a cylindrical symmetry on the electronic wave functions but keeps an explicit ionic structure in full 3D. In such calculations, the laser polarization is along the symmetry axis, while in full 3D calculations, it can take any directions. The electronic ground state is determined by the damped gradient method [18]. Time propagation of the Kohn-Sham (KS) wave functions is done with the time-splitting method [19]. Absorbing boundary conditions are used to remove outgoing electrons at the boundaries of the numerical box [20]. The net ionization ($N_{\rm esc}$) is approximately calculated as the difference between the number of electrons in ground state ($N_{\rm el}$) and that left in the box after laser pulse is over, expressed as [21] $N_{\rm esc}(t) = N_{\rm el} - \int {\rm d}^3\mathbf{r}\, \rho(\mathbf{r},t)$, where $\rho(\mathbf{r},t)$ is the time-dependent electronic density built from the KS wave functions. The electronic dipole moment is defined as $\mathbf{D}(t) = \int {\rm d}^3\mathbf{r}\, \rho(\mathbf{r},t)\, \mathbf{r}$, and characterizes the electronic response of the system in time.

3. Results

3.1. Impact of laser polarization and ionic motion

We first perform a scan on delay time $\Delta\tau$, at the fixed XUV frequency $\omega_{\rm atto} = 35$ eV, much larger than the ionization potential (IP) of N_2 at -$\varepsilon_{\rm HOMO} = 16.1$ eV, where it is assumed that the

negative highest occupied molecular orbital (HOMO) energy ($\varepsilon_{\mathrm{HOMO}}$) is equal to the vertical IP according to the Koopmans' theorem [22]. Therefore, each XUV attopulse can easily promote an electron from the bound states into the continuum. The NIR pulse, although strong, has a frequency far below the IP and can hardly produce ionization alone. The lower panel of Fig. 1 shows the dipole signal of the underlying NIR pulse during the time window when APT is introduced by the delay time $\Delta\tau$. It follows quasi-statically the NIR field thus oscillating with

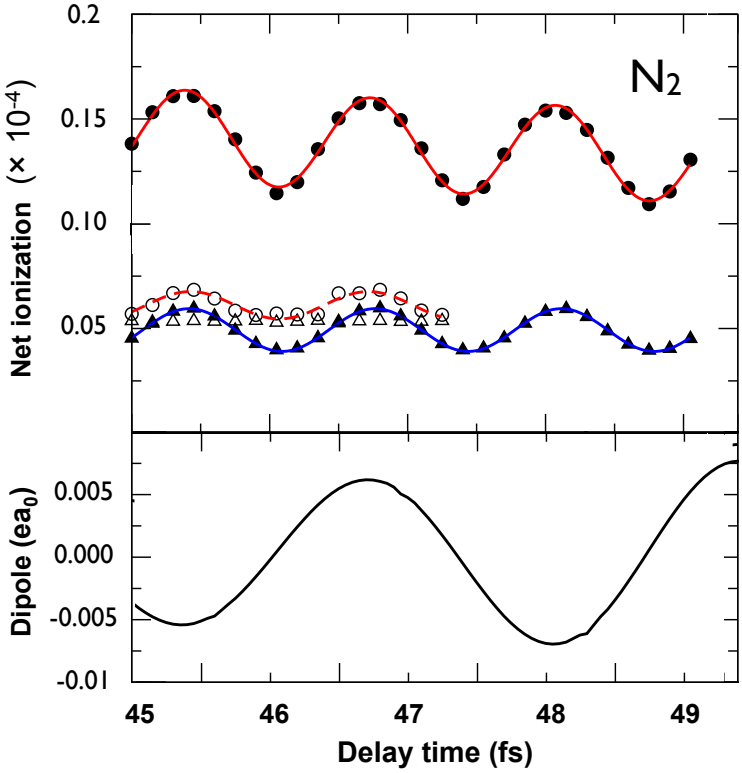

Figure 1. Key observables as functions of delay time $\Delta\tau$ for a N_2 molecule irradiated by a combined NIR and XUV APT, as described in section 2, with $\omega_{\mathrm{atto}} = 35$ eV. Lower panel: electronic dipole moment along the N_2 molecule. Upper panel: net ionization with frozen ions (close symbols) and moving ions (open symbols), obtained for a laser polarization along the N_2 molecular axis (circles) or perpendicular to it (triangles). Curves are drawn through the symbols to guide the eye.

ω_{NIR}. The upper panel shows the net ionization for 4 different cases, that is a laser polarization along (circles) or perpendicular (triangles) to the N_2 molecular axis, and with frozen (close symbols) or moving (open symbols) ions. All cases show more or less pronounced oscillations with $\Delta\tau$. Those oscillation patterns with a periodicity of $T_{\mathrm{NIR}}/2$ were observed earlier and explained by time-dependent localization of the electrons in N_2 molecule [15], resulting from the screening of the XUV laser field in a polarized N_2 molecule.

In relation to the induced dipole (lower panel), we find that maxima of N_{esc} correspond to the largest dipole moments, while minima of N_{esc} correlate with nodal points of the dipole signal. For the cases with frozen ions, we observe that the aligned laser pulse produces more ionization than the laser polarized perpendicular to the molecular axis. This is expected since the dipole

moment is more responsive along the molecular axis than in the perpendicular one.

The overall pulse length $T_{\rm NIR} = 60$ fs is much larger than the 14.14 fs period of N_2 vibrations. To explore the role of ionic vibrations, we compare the results obtained with frozen ions to those with moving ions. The (more expensive) simulations are performed on a smaller, yet sufficient, set of delay times, just covering one NIR period. Ionic motion dramatically limits the electron yield by a factor of 3 for the aligned laser polarization, and also strongly reduces the amplitude of the oscillations. The net ionization effect is less dramatic for the perpendicular polarization but the amplitude vanishes almost completely. These reductions of oscillation by the ionic motion can be explained by the fact that the molecular modes do not match the repetition times of the external laser field, thus spoiling the phase relations which are needed to enhance electron emission. The nearly full suppression of the oscillations in the perpendicular case is probably due to the triggering of large molecular rotations that can perturb the response even more.

3.2. Dependence on XUV frequency

We now study the impact of the XUV attopulse frequency $\omega_{\rm atto}$ on the electron emission. A variety of frequencies are used, well below threshold (we remind that IP=16.1 eV), close to threshold, and well above. For such a scan, computations in full 3D are too expensive. Therefore, the calculations have been performed in the CAPS and with frozen ions. The laser polarization is fixed along the molecular axis. Figure 2 shows the net ionization as a function of the delay time $\Delta\tau$. One can notice that the net ionization obtained by 2D scheme is roughly a factor of 2 larger than that calculated from 3D calculations under the similar laser conditions, i.e., at 34 eV in Fig. 2 and the toppest curve in Fig. 1. This is not surprising because the net ionization varying with delay time of APT is associated with NIR laser pulse [15], the closer to the maximum of NIR laser field ($T_{\rm NIR}/2$= 30 fs) the delay time, the larger the net ionization. Figure 2 reveals

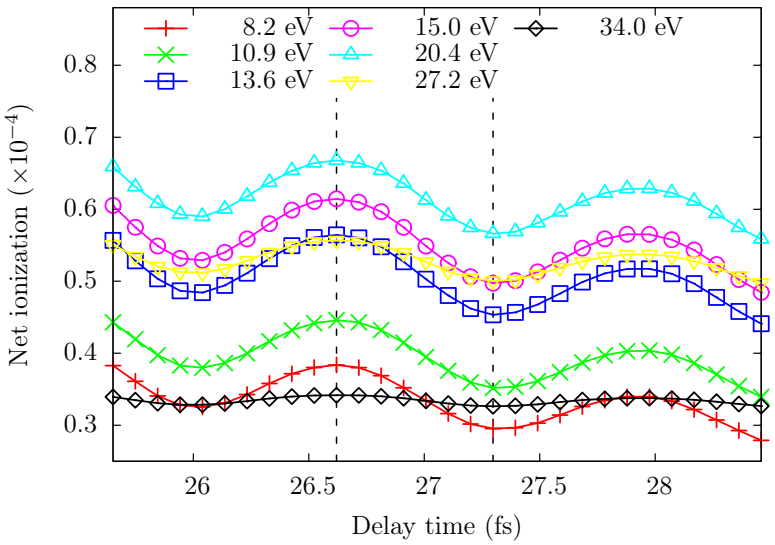

Figure 2. Net ionization as a function of delay time from N_2 irradiated by a combined NIR and XUV APT with frozen ions and in the CAPS (see section 2). Different XUV attopulse frequencies are used as indicated by various symbols. The dashes emphasize the maxima and minima.

that all frequencies produce qualitatively the same oscillation pattern with a period of $T_{\rm NIR}/2$, and with all maxima and minima located at the same $\Delta\tau$. However, for $\omega_{\rm atto}$ smaller than the ionization threshold, excited states can be attained. And considering the finite width of the APT

(about $5-10$ eV), the matching of laser frequencies delivered by the APT with eigenfrequencies of N_2 is expected to blur or to change the ionization pattern. This is not what we observe, since the ionization oscillations all look independent of $\omega_{\rm atto}$. This result is also at variance with the calculations of Rivière *et al* [23] using the strong field approximation (based on the assumption of a single-active electron) and for the He atom. They found two limiting cases. The first one is for $\omega_{\rm atto}$ <IP : the maxima of ionization occur at the times for which the NIR dipole is maximal, and the minima when the NIR dipole vanishes. The second case is for $\omega_{\rm atto}$ >IP+$2U_{\rm p}$, where $U_{\rm p}$ is the pondermotive energy. Here, $U_{\rm p}$=0.06 eV, thus negligible. According to the findings of [23], at the delay time for extrema there should occur maxima (minima) and minima (maxima) for two distinct cases, respectively. Our calculations, on the contrary, do not exhibit such a reverse behavior, since the maxima and minima are found for the same $\Delta\tau$, whatever the value of $\omega_{\rm atto}$ with respect to IP. This indicates that the single-active-electron approximation is probably not applicable in such a multielectron system as N_2. In particular, strong polarization effects in N_2 might play an important role in the electron emission.

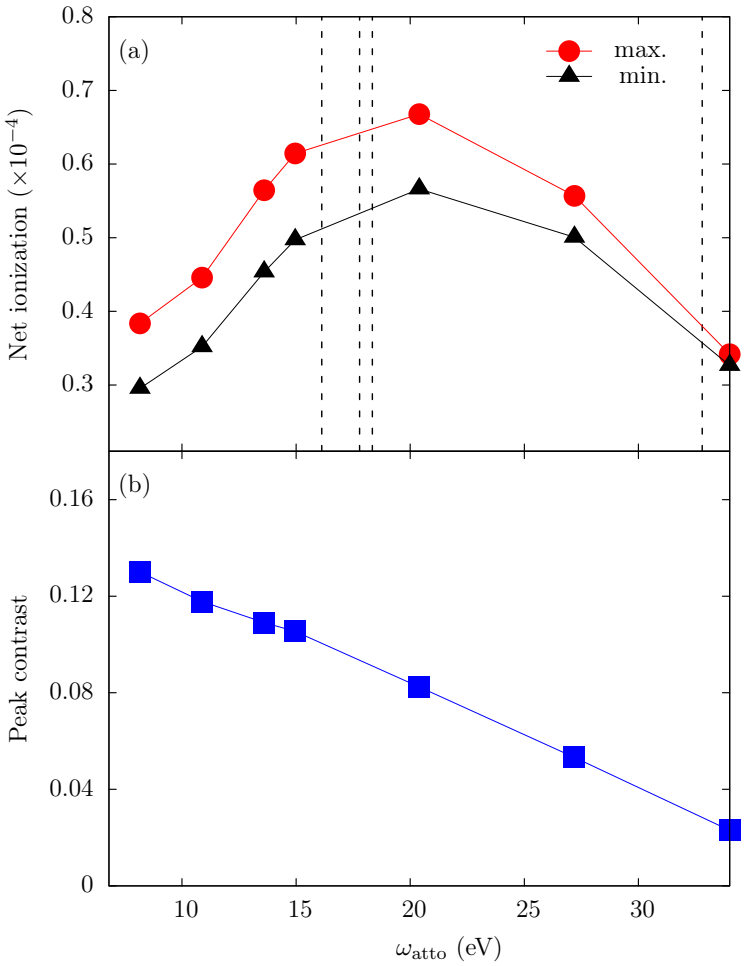

Figure 3. (a) Net ionization as a function of XUV frequency $\omega_{\rm atto}$, deduced from Fig. 2. Circles: maxima of ionization ($N_{\rm esc}^{\rm max}$) at $\Delta\tau$ = 26.62 fs. Triangles : minima ($N_{\rm esc}^{\rm min}$) at $\Delta\tau$ = 27.3 fs. The dashed vertical lines are positioned at the absolute value of the single-electron energies of N_2, see the main text. (b) Peak contrast between maximum and minimum of ionization, defined as $P = \frac{N_{\rm esc}^{\rm max}-N_{\rm esc}^{\rm min}}{N_{\rm esc}^{\rm max}+N_{\rm esc}^{\rm min}}$.

Figure 2 also shows marked changes in the amplitude with the XUV frequency. To better vizualize these changes, we select two delay times, namely $\Delta\tau = 26.62$ fs corresponding to a maximum of yield, and $\Delta\tau = 27.3$ fs corresponding to a minimum. The net ionization at these two instants is drawn as a function of the XUV frequency $\omega_{\rm atto}$ in panel (a) of Fig. 3. In order to illustrate the variation of net ionization with $\omega_{\rm atto}$, the absolute value of calculated single-electron energies of N_2 is marked by dashed lines in ascending order as 16.1 eV, 17.8 eV, 18.3 eV, and 32.8 eV. It is found that the frequency dependence of the maximum is very similar to that of the minimum. They both increase with $\omega_{\rm atto}$, reach a maximum around 20 eV, and then decrease. These behaviors are consistent with multi-photon processes for $\omega_{\rm atto} <$ IP, with a larger ionization as soon as $\omega_{\rm atto}$ comes closer to the IP (less and less photons are required), and with one-photon processes for $\omega_{\rm atto} >$ IP where the effective field strength goes down as $\omega_{\rm atto}^{-2}$, according to the Keldysh parameter [24].

A further interesting quantity is the peak contrast defined as $P = \dfrac{N_{\rm esc}^{\rm max} - N_{\rm esc}^{\rm min}}{N_{\rm esc}^{\rm max} + N_{\rm esc}^{\rm min}}$. It is shown in panel (b) of Fig. 3 as a function of $\omega_{\rm atto}$. We observe a steady decreases of the contrast. In other words, the larger XUV frequency, the less visible the oscillatory pattern. In the studied frequency window, the decrease follows approximately a linear trend. The most remarkable contrast in the present study are seen at the lowest frequency 8.2 eV (reaching 13%), while the weakest signal with a contrast of only 2.3% occurs at the largest frequency 34 eV. We remind that the attopulse intensity and the duration of individual pulse are kept constant in this frequency scan. At very high $\omega_{\rm atto}$, ionization as such has no time to set in and therefore, to be sensitive to the delay time. Mind also that the absolute values of the ionization are very small ($< 10^{-4}$).

4. Conclusions

In this contribution, we have studied from a theoretical perspective trends of ionization from a N_2 molecule after the irradiation by an external laser field constructed from the combination of a near-infrared (NIR) pulse and a train of attosecond XUV pulses (APT). This is a typical set-up in recent experiments aiming at time-resolved measurements of electron dynamics in small molecules. The measurements show a strong dependence of ionization on the delay time between the NIR pulse and the APT.

We have simulated the electronic dynamics by means of time-dependent density-functional theory augmented by a self-interaction correction and optionally coupled to molecular dynamics for the molecule ions. The laser pulse parameters have been chosen according to the aforementioned experiments. The calculations confirm the appearance of marked oscillations in the net ionization with delay time separated by half a period of the NIR pulse. We found that the maximum of yield is always correlated with the extremum of the dipole signal (from the response to NIR field). The electron emission is larger in case of frozen ions than in the case of moving ions, which corresponds to the realistic scenario for experiments in the gas phase. The laser polarization aligned with the molecular axis also delivers a higher ionization, compared with the case of a perpendicular polarization. The amplitude of the oscillations with delay time shows marked trends: it increases with XUV frequency for frequencies below ionization threshold, and decreases for frequencies above, having therefore a maximum near threshold. The contrast of the yield (relative amplitude) decreases monotoneously with XUV frequency.

The present study shows that there are indeed robust time-resolved signals in the electronic emission induced by the NIR-APT setup. Some of the observed trends are consistent with expected behaviors. However, other trends need more analysis to be clearly explained. Work in this direction is in progress.

5. Acknowledgments

C.-Z.G. is grateful to the financial support from China Scholarship Council (CSC) (No. [2013]3009). We thank Institut Universitaire de France, European ITN network CORINF and French ANR contract MUSES for support during the realization of this work. It was also granted access to the HPC resources of CalMiP (Calcul en Midi-Pyrénées) under the allocation P1238, and of RRZE (Regionales Rechenzentrum Erlangen).

References

[1] Zewail A H 1994 *Femtochemistry: ultrafast dynamics of the chemical bond* vol 1 (World Scientific)
[2] Paul P M, Toma E, Breger P, Mullot G, Augé F, Balcou P, Muller H and Agostini P 2001 *Science* **292** 1689–1692
[3] Johnsson P, López-Martens R, Kazamias S, Mauritsson J, Valentin C, Remetter T, Varjú K, Gaarde M B, Mairesse Y, Wabnitz H, Salières P, Balcou P, Schafer K J and L'Huillier A 2005 *Phys. Rev. Lett.* **95**(1) 013001
[4] Johnsson P, Mauritsson J, Remetter T, L'Huillier A and Schafer K J 2007 *Phys. Rev. Lett.* **99**(23) 233001
[5] Krausz F and Ivanov M 2009 *Rev. Mod. Phys.* **81**(1) 163–234
[6] Kelkensberg F, Siu W, Pérez-Torres J F, Morales F, Gademann G, Rouzée A, Johnsson P, Lucchini M, Calegari F, Sanz-Vicario J L, Martín F and Vrakking M J J 2011 *Phys. Rev. Lett.* **107**(4) 043002
[7] Kulander K C, Schafer K J and Krause J L 1992 Time-dependent studies of multiphoton processes *Atoms in intense laser fields*
[8] Runge E and Gross E K U 1984 *Phys. Rev. Lett.* **52** 997
[9] Calvayrac F, Reinhard P G, Suraud E and Ullrich C A 2000 *Phys. Rep.* **337** 493
[10] Perdew J P and Wang Y 1992 *Phys. Rev. B* **45** 13244
[11] Legrand C, Suraud E and Reinhard P G 2002 *J. Phys. B* **35** 1115
[12] Wopperer P, Dinh P M, Reinhard P G and Suraud E 2015 *Phys. Rep.* **562** 1
[13] Goedecker S, Teter M and Hutter J 1996 *Phys. Rev. B* **54** 1703
[14] Gao C Z, Dinh P, Reinhard P G and Suraud E 2015 *Ann. Phys.* **360** 98 – 112
[15] Neidel C, Klei J, Yang C H, Rouzée A, Vrakking M J J, Klünder K, Miranda M, Arnold C L, Fordell T, L'Huillier A, Gisselbrecht M, Johnsson P, Dinh M P, Suraud E, Reinhard P G, Despré V, Marques M A L and Lépine F 2013 *Phys. Rev. Lett.* **111**(3) 033001
[16] Reinhard P G and Suraud E 2003 *Introduction to Cluster Dynamics* (New York: Wiley)
[17] Montag B and Reinhard P G 1994 *Phys. Lett. A* **193** 380
[18] Reinhard P G and Cusson R Y 1982 *Nucl. Phys. A* **378** 418
[19] Feit M D, Fleck J A and Steiger A 1982 *J. Comp. Phys.* **47** 412
[20] Reinhard P G, Stevenson P D, Almehed D, Maruhn J A and Strayer M R 2006 *Phys. Rev. E* **73** 036709
[21] Ullrich C A 2000 *J. Mol. Struct. (THEOCHEM)* **501-502** 315
[22] Koopmans T 1934 *Physica* **1** 104–113
[23] Rivière P, Uhden O, Saalmann U and Rost J M 2009 *New J. Phys.* **11** 053011
[24] Keldysh L V 1965 *Sov. Phys. JETP* **20** 1307